Journal of Inorganic Biochemistry 199 (2019) 110784

Contents lists available at ScienceDirect

Journal of Inorganic Biochemistry

journal homepage: www.elsevier.com/locate/jinorgbio

Polyoxometalates: Study of inhibitory kinetics and mechanism against α-glucosidase

Guoxiang Chi[a], Li Wang[a,*], Bingnian Chen[b,*], Jian Li[a], Jingjing Hu[a], Shuxia Liu[c,*], Meijuan Zhao[a], Xiaomei Ding[a], Yue Li[a]

[a] College of Food and Biological Engineering, Jimei University, Xiamen 361021, PR China
[b] Xiamen University Hospital, Xiamen 361005, PR China
[c] Key Laboratory of Polyoxometalate Science of Ministry of Education, College of Chemistry, Northeast Normal University, Changchun, Jilin 130024, PR China

ARTICLE INFO

Keywords:
Polyoxometalates
α-Glucosidase inhibitors
Enzyme kinetics
Molecular docking

ABSTRACT

Alpha-glucosidase is considered to be an important target for the treatment of noninsulin-dependent diabetes. In this work, the inhibitory effects of polyoxometalates (POMs) affected by three different factors (heteroatom, transition metal substitution element and vanadium substitution number) on α-glucosidase were studied. We found that POMs with Keggin-type and vanadium-substituted Dawson-type structures act as effective and mostly competitive inhibitors for α-glucosidase (IC_{50} values around 40–160 μM), and most compounds can compete with the substrate for the active site of α-glucosidase. By analyzing and comparing the inhibitory effects of each series of POMs on α-glucosidase, the results demonstrated that the structure and composition of the POMs themselves may indirect influence on their inhibitory capabilities. Moreover, we gained initial information about the structure-inhibition relationship of different POMs. More intriguingly, molecular docking simulation suggested that all compounds bind into the active site of α-glucosidase by multiple van-der-Waals and hydrogen bond interactions. Our kinetic data demonstrate the considerable potential of POMs for the development of clinically valuable α-glucosidase inhibitors.

1. Introduction

Type 2 diabetes (non-insulin-dependent diabetes) is a type of a chronic hyperglycemia disorder caused by insulin deficiency or insulin resistance [1,2]. α-Glucosidase is a carbohydrate hydrolase which is considered to be an important target for the treatment of non-insulin-dependent diabetes mellitus [3]. In recent years, the development of safe and effective α-glucosidase inhibitors has become a hotspot of research for the treatment of non-insulin-dependent diabetes mellitus. Peng et al. [4] reported that kaempferol showed a notable inhibition activity on α-glucosidase. Taha et al. [5] designed and synthesized seventeen Coumarin based derivatives that showed outstanding α-glucosidase inhibitory potential many folds better than the standard acarbose. However, the reported research on α-glucosidase inhibitors mainly focuses on natural extracts and organic compounds, and few inorganic agents have been reported that can inhibit α-glucosidase. Moreover, the current therapeutic drugs (acarbose [6], miglitol [7] and voglibose [8]) on the market are incompletely satisfactory due to the high cost and toxic side effects (Table S1). Therefore, the design of high efficiency, low cytotoxicity and low cost α-glucosidase inhibitors is an attractive goal in the field of medicinal chemistry.

Polyoxometalates (abbreviated as POMs), due to their incomparable structural diversity, novel functional properties and multifaceted bioactivities, have shown good application prospects that encompasses anticancer [9–12], antiviral [10,13], antibacterial [14,15], against Alzheimer's disease [16–18] and enzyme inhibition [19–22] in the field of medicine. Many studies have validated that POMs possess significant inhibitory effects on the activities of kinase, nucleotidase, phosphatase, sialyltransferase, nuclease, sulfotransferase, acetylase and protease [23]. Gumerova et al. [24] studied the inhibitory effects of nine different polyoxotungstates (POTs) on P-type ATPases in vitro (Ca^{2+}-ATPase) and ex vivo (Na^+/K^+-ATPase), and the results reveal some POTs are potent ATPase inhibitors, with $K_9(C_2H_8N)_5[H_{10}Se_2W_{29}O_{103}]$ showing high selectivity toward Ca^{2+}-ATPase. Moreover, the information about POMs as anti-diabetic agents is rapidly increasing in the last 30 years thereby creating many highlights (see Scheme S1). We found that the research of scientists is mainly focused on the anti-diabetic effect of vanadate [25,26] and tungstate [25,27]. Most recently, our group has reported that the $H_3PMo_{12}O_{40}$ and three transition metal-substituted Keggin-type phosphomolybdic acids can be excellent

* Corresponding authors.
E-mail addresses: wanglimerry@jmu.edu.cn (L. Wang), wanglimerry@xmu.edu.cn (B. Chen), liusx@nenu.edu.cn (S. Liu).

https://doi.org/10.1016/j.jinorgbio.2019.110784
Received 11 May 2019; Received in revised form 13 July 2019; Accepted 15 July 2019
Available online 17 July 2019
0162-0134/

inhibitors to α-glucosidase activity, and the $H_3PMo_{12}O_{40}$ possess the strongest inhibition effect [28]. However, the structure-activity relationship of POMs and fundamental questions regarding the binding mode of POMs inhibitors on enzymes is largely unknown, especially for α-glucosidase. In addition, POMs are characterized by species diversity, structural modification, and extensive inhibition of enzymes. Therefore, the screening of a large number of POMs, especially of the Keggin and Dawson-type with superior inhibitory properties and lower cytotoxicities [29–32] may result in clinically valuable α-glucosidase inhibitor drugs.

Herein, the primary focus of this paper is to present the Keggin-type and vanadium-substituted Dawson-type POMs (Fig. S1) with potential pharmacological activity on α-glucosidase. Three structural crucial factors of POMs - heteroatom, transition metal substitution element and vanadium substitution number - have been varied and the corresponding inhibition kinetics performed. Importantly, we initially analyzed the structure-inhibition relationship of POMs and fundamental questions regarding the mechanisms of the inhibitory capabilities of POMs on α-glucosidase. This work provides an enlightened strategy for the in-depth study of polyoxometalate medicinal chemistry and designing novel, safe and effective α-glucosidase inhibitors.

2. Materials and methods

2.1. Reagents

$H_5GaMo_{12}O_{40}$ [33], $H_4SiMo_{12}O_{40}$ [34], $Na_7PMo_{11}MO_{40}$ (M = Ni, Mn, Zn, Cr) [35,36] and $H_{6+n}P_2Mo_{18-n}V_nO_{62}$ (n = 1–5) [37,38] (abbreviated as $GaMo_{12}$, $SiMo_{12}$, $PMo_{11}M$ and $P_2Mo_{18-n}V_n$, respectively) were synthesized as previously described with slight modifications. Next, the structure of the synthetic compounds was characterized by IR (Jasco FT/IR-480) and UV/*Vis* (Cary-50) spectroscopy. Moreover, the structure of $P_2Mo_{18-n}V_n$ (n = 1–5) were further characterized by solid nuclear magnetic resonance spectrometry (UNITY + -300). α-Glucosidase of *S. cerevisiae* (EC 3.2.1.20), *p*-Nitrophenyl-α-D-glucopyranoside (*p*NPG), *p*-Nitrophenol (*p*NP) and Dimethyl sulfoxide (DMSO) were purchased from Sigma-Aldrich Chemical Co. (USA). All other reagents were locally sourced and of analytical grade, and the ultra-pure water was used throughout.

2.2. Experiment procedure

2.2.1. Enzyme kinetics analysis

In this experiment, *p*NPG was used as a substrate to generate a yellow product (*p*NP) with catalysis by α-glucosidase, and the OD value after the reaction of the system was monitored by the microplate reader (Synergy H1) at a wavelength of 405 nm [28]. Briefly, the reaction system was sequentially supplemented with 133 μL of 0.1 M phosphate buffer (Na_2HPO_4-NaH_2PO_4 buffer, pH 6.8), 7 μL of different concentrations of inhibitors completely dissolved in DMSO solution (the final concentration of DMSO in the test solution was 5%), and 10 μL of α-glucosidase solution that was added immediately. Next, the mixture was incubated at 37.0 °C for 10 min, and 20 μL of the substrate (*p*NPG) preheated at 37.0 °C for 10 min was added to the mixture. The reaction was carried out at 37.0 °C for 20 min, and then the reaction was terminated by the addition of an equal volume of Na_2CO_3 solution (1 M). The OD value of the 200 μL reaction solution was monitored in a 96-well plate by using the microplate reader at 405 nm [28]. As previously described [28], the inhibitory effect (IC_{50}), inhibition mechanism and inhibition type of three different factors (heteroatom, transition metal substitution element and vanadium substitution number) of POMs on α-glucosidase were studied.

2.2.2. Molecular docking study

To predict the binding mode of each series of synthesized compounds with α-glucosidase, a molecular docking study was carried out using MOE (Molecular Operating Environment) software package. According to our previous report [28,39], the three-dimensional structures of the synthesized compounds were generated via using the builder tool in MOE. The generated compound was 3D protonated and energy minimized using the default parameters of the MOE (gradient: 0.05, Force Field: MMFF94X, pH 6.8). These compounds were then saved into an mdb file for further evaluation.

However, the 3D structure for α-glucosidase of *S. cerevisiae* has not been solved yet. The template structure; Herein, the crystal structure of isomaltase from *S. cerevisiae* (PDB 3AJ7) share 82% homology with the *S. cerevisiae* α-glucosidase, which is generally as considered excellent value for the selection of template [40]. Moreover, the homology modeling process of α-glucosidase and the details, and parameters of molecular docking in this paper, are the same as those of previously described [28,41].

2.2.3. Statistical analysis

The experimental data were repeated five times under parallel determination by using SPSS version 17.0 and GraphPad Prism version 7.0 for analysis. Experimental drawings were completed using Origin 8.0 professional software. Error bars indicate ± s.d.

3. Results and discussion

3.1. Analysis of Keggin-type POMs with different kinds of central atoms (heteroatom)

3.1.1. Spectroscopic characterization

Table S2 listed the IR spectra and the UV–*Vis* spectra data of the compounds $GaMo_{12}$ and $SiMo_{12}$. In the IR spectra, the two compounds showed most characteristic bands at 700–1100 cm^{-1} due to molybdenum-oxygen stretching vibrations. In the UV–*Vis* spectra, the compounds showed two characteristic absorption bands at 195 nm and 310 nm, respectively. The data in the table strongly indicated that these two complexes have Keggin-type structures, which is consistent with the results of references [33, 34].

3.1.2. The inhibitory effect of compounds on α-glucosidase

To compare the inhibitory effects of POMs with different central atoms on α-glucosidase, we selected compounds $GaMo_{12}$ and $SiMo_{12}$ as inhibitors to study the effect of POMs on the activity of α-glucosidase-catalyzed *p*NPG. As shown in Fig. S2, the α-glucosidase activity revealed a significant decrease with increased the concentrations of the inhibitors ($GaMo_{12}$ and $SiMo_{12}$). The concentrations of $GaMo_{12}$ and $SiMo_{12}$ when the α-glucosidase activity was decreased by 50% (IC_{50}) were 615.10 ± 17.00 μM and 33.71 ± 0.76 μM, respectively. Compared with our previously reported PMo_{12} [28], the inhibitory effects of these three Keggin-type POMs are $GaMo_{12}$ < $SiMo_{12}$ < PMo_{12}. From the above results, the IC_{50} revealed a significant decrease with increased the heteropolyanions charge (Ga: −3, Si: −4 and P: −5), which indicated a significant indirect influence of the central atom charge on the inhibition behaviour. In addition, the acid strength of POMs were determined by alkaline method as $GaMo_{12}$ < $SiMo_{12}$ < PMo_{12}, and studies have shown that the oxidizability of Keggin-type POMs with the same structure are mainly affected by the electrostatic effect of the anionic charge, which decreases with the oxidation state of the central atom, and its oxidizability decreases as the negative charge of the POMs increases [42,43]. Based on the above theory, we found that the different central atomic species of POMs change their own redox property and acidity, which may cause significant differences in the inhibition behaviour of the three POMs on α-glucosidase. We also found that the inhibitory effects of $GaMo_{12}$ and $SiMo_{12}$ on α-glucosidase were less effective than those of PMo_{12}, but the inhibitory effects of these two inhibitors were more significant than those of standard commercial acarbose (IC_{50} = 750 ± 1.5 μM) [44]. Among them, the inhibitory strength of $SiMo_{12}$ is approximately 23

times higher than that of acarbose.

In addition, we also studied the inhibitory mechanism and inhibitory type of inhibitors on α-glucosidase activity. The results are shown in Table 1. From Fig. S3, in the reaction system, the plots of the remaining enzyme activity versus the concentrations of the enzyme produced several adjacent straight lines, which all passed through the origin. Next, a linear decrease with increasing concentrations of inhibitors indicated that the inhibition mechanisms of these two inhibitors on α-glucosidase were reversible [28,45]. Therefore, these two inhibitors are non-covalently attached to the active center of the enzyme by multiple polar and non-polar interactions. Moreover, the inhibition type of the $GaMo_{12}$ and $SiMo_{12}$ on the α-glucosidase activity was determined using the Lineweaver-Burk (double-reciprocal) plots of the reciprocal of the reaction rate versus the reciprocal of the substrate concentration. The inhibitory constant (K_I or K_{IS}) of the inhibitors was further calculated through secondary mapping, and the results are shown in Fig. S4. As shown in Fig. S4, the graph of $1/v$ versus $1/[s]$ represented a set of straight lines which all intersected at or extremely close to the Y-axis. Next, the linear slope increased gradually as the concentrations of the $GaMo_{12}$ and $SiMo_{12}$ inhibitors increased, while the vertical axis intercept remained unchanged, which suggested that the inhibitors compete with the substrate for the active site of the α-glucosidase [45]. Furthermore, the inhibitory constants K_I of the $GaMo_{12}$ and $SiMo_{12}$ were calculated by further plotting the linear slopes versus the inhibitor concentrations of 0.630 mM and 0.032 mM, respectively.

3.1.3. Analysis of molecular docking results

Different inhibitory effects on the target protein may occur due to differences in the chemical structure or the mechanism of action of the inhibitor itself. To vividly represent the binding forms and interactions of the ligands ($GaMo_{12}$ and $SiMo_{12}$) in the active site of α-glucosidase, the experimental results were analyzed by the MOE (Fig. 1AB) and the PyMOL (Fig. 1CD) software. As shown in Fig. 1AB, the amino acid residues surrounding the compound are represented by pink and green circles. $GaMo_{12}$ and $SiMo_{12}$ accurately fit into the deep pocket of the active site and is largely surrounded by the polypeptide. After docking scoring, the scores for $GaMo_{12}$ and $SiMo_{12}$ docking with α-glucosidase were −11.68 and −13.62 kcal/mol, respectively. The score meant that the docking of these two compounds with α-glucosidase was successful. In addition, the smaller the numerical value is, the better is the ability of the compound to bind to the biomacromolecule. Therefore, in combination with the previous report [28], the binding ability of the compound to α-glucosidase is $GaMo_{12} < SiMo_{12} < PMo_{12}$ (Table S3). Further molecular docking study validated the experimental results of the enzyme kinetics.

Furthermore, as shown in Fig. 1, $SiMo_{12}$ forms five hydrogen bonds with the amino acid residues (Ser240, His280, Pro312 and Arg315) in the active region, while $GaMo_{12}$ forms only three hydrogen bonds with the amino acid residues (Ser240 and Asp242) in the active region (Table S3), so the inhibition of $SiMo_{12}$ is greater than that of $GaMo_{12}$. Similarly, the inhibition of PMo_{12} is greater than that of $SiMo_{12}$ and $GaMo_{12}$. In addition to the hydrogen bonding interactions with the enzyme, the compounds also form several van der Waals interactions which significantly contribute to the strong binding of the compounds. However, we found no significant difference in the number of amino acid residues involved in van der Waals interactions among the three compounds. According to the molecular simulation, the $SiMo_{12}$ and

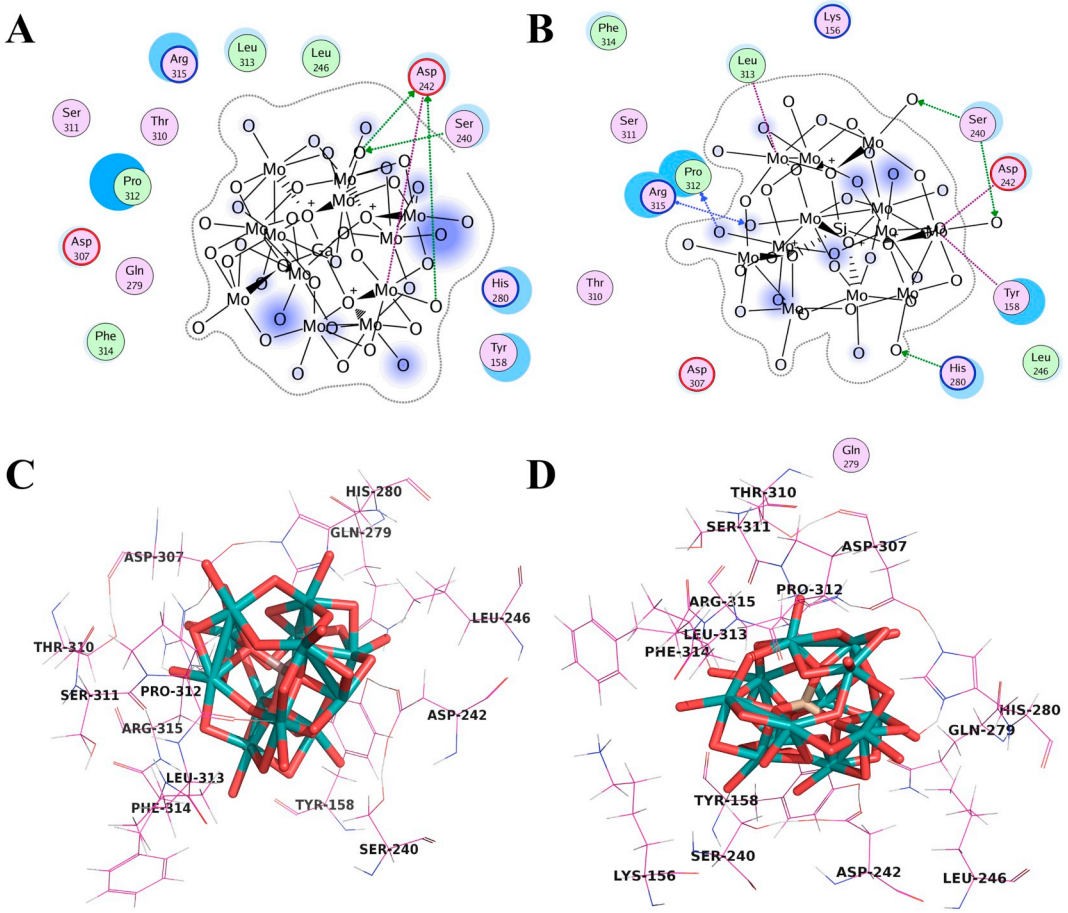

Fig. 1. Docking conformations of ligand $GaMo_{12}$ and $SiMo_{12}$ in α-glucosidase. Two-dimensional ligand interaction map of compounds $GaMo_{12}$ (A) and $SiMo_{12}$ (B) docked into the binding site of α-glucosidase; three-dimensional complex interaction of α-glucosidase and the ligands $GaMo_{12}$ (C) and $SiMo_{12}$ (D).

Table 1
Enzyme kinetic results of all synthetic compounds on α-glucosidase. Error bars indicate ± s.d.

Compound (POMs)	IC_{50}/(μmol·L^{-1})	Inhibitory mechanism	Inhibitory type	Inhibitory constant		Ref.
				K_I/(mmol·L^{-1})	K_{IS}/(mmol·L^{-1})	
$H_5GaMo_{12}O_{40}$	615.10 ± 17.00	Reversible	Competitive	0.630		
$H_4SiMo_{12}O_{40}$	33.71 ± 0.76	Reversible	Competitive	0.032		
$H_3PMo_{12}O_{40}$	6.41 ± 0.38	Reversible	Competitive	0.018		[19]
$Na_7PMo_{11}NiO_{40}$	37.29 ± 1.72	Reversible	Mixed-type	0.049	0.109	
$Na_7PMo_{11}MnO_{40}$	47.66 ± 1.15	Reversible	Competitive	0.079		
$Na_4PMo_{11}VO_{40}$	52.33 ± 1.41	Reversible	Competitive	0.146		[19]
$Na_7PMo_{11}ZnO_{40}$	99.23 ± 2.24	Reversible	Competitive	0.059		
$Na_7PMo_{11}CoO_{40}$	103.10 ± 2.88	Reversible	Competitive	0.121		[19]
$Na_7PMo_{11}CrO_{40}$	126.20 ± 3.70	Reversible	Competitive	0.278		
$Na_6PMo_{11}FeO_{40}$	161.90 ± 7.68	Reversible	Noncompetitive	0.312	0.412	[19]
$H_7[P_2Mo_{17}VO_{62}]$	164.20 ± 14.20	Reversible	Competitive	0.328		
$H_8[P_2Mo_{16}V_2O_{62}]$	117.40 ± 3.64	Reversible	Competitive	0.278		
$H_9[P_2Mo_{15}V_3O_{62}]$	57.01 ± 2.11	Reversible	Competitive	0.024		
$H_8[P_2Mo_{14}V_4O_{62}H_2]$	127.13 ± 4.01	Reversible	Competitive	0.110		
$H_9[P_2Mo_{13}V_5O_{62}H_2]$	99.65 ± 2.45	Reversible	Competitive	0.053		

$GaMo_{12}$ do bind to the enzyme active groups in the form of hydrogen bonding and van der Waals interactions. Therefore, the catalytic group of the enzyme is generally not destroyed, and the enzyme is not inactivated, which proves that both compounds are a reversible inhibitor [28].

3.2. Analysis of different transition metal-substituted Keggin-type POMs

3.2.1. Spectroscopic characterization

Table S4 listed the IR spectra (four characteristic bands at 700–1100 cm^{-1}) and the UV–*Vis* spectra (two characteristic absorption bands at 200 nm and 260 nm) data of the compounds $PMo_{11}M$ (M = Ni, Mn, Zn, Cr). These data in the table strongly indicated that these complexes have Keggin-type structures, which is consistent with the results of references [35, 36]. Among them, the peak positions of the compounds in the table were shifted, which may be due to the substitution of transition metals.

3.2.2. The inhibitory effect of compounds on α-glucosidase

To compare the effects of different transition metal-substituted Keggin-type POMs on α-glucosidase, four transition metal-substituted Keggin-type POMs were synthesized and used as inhibitors to study their inhibitory effects on α-glucosidase. As shown in Fig. S5, the α-glucosidase activity gradually decreased as the concentration of the inhibitors $PMo_{11}M$ (M = Ni, Mn, Zn, Cr) increased. Compared with the previously studied inhibitors ($PMo_{11}V$, $PMo_{11}Co$ and $PMo_{11}Fe$) [28], the inhibitory effects of the seven Keggin-type POMs on α-glucosidase were $PMo_{11}Fe$ < $PMo_{11}Cr$ < $PMo_{11}Co$ < $PMo_{11}Zn$ < $PMo_{11}V$ < $PMo_{11}Mn$ < $PMo_{11}Ni$. Next, compared with standard acarbose (IC_{50} = 750 ± 1.5 μM) [44], the inhibition potency of $PMo_{11}Ni$ (IC_{50} = 37.29 ± 1.72 μM) was approximately 20 times higher than that of acarbose, so the synthesized inhibitors in our laboratory possess significant inhibitory effects on α-glucosidase. It was revealed that, as compared to the IC_{50} of each compound, we found that the inhibitory effects of the three compounds ($PMo_{11}Ni$, $PMo_{11}Mn$ and $PMo_{11}V$) on α-glucosidase were generally much stronger than the other four, which may be mainly due to the substitution of metal elements of POMs to α-glucosidase has different inhibition behaviour. The substitution of different transition metal elements may also change their own redox properties, which may indirect influence the inhibition behaviour of the POMs on α-glucosidase, and the need for further research is emphasized. Moreover, the reason why the inhibitory effect of $PMo_{11}Fe$ on α-glucosidase is worse than other compounds may be that its inhibition type is different from others. Similarly, the inhibition mechanism of the four compounds we synthesized was all reversible (Fig. S6). Except that $PMo_{11}Ni$ showed mixed-type inhibition, the inhibition types of the other three compounds were all competitive (Fig. S7). In the mixed-type inhibition, the inhibitor $PMo_{11}Ni$ can affect the affinity of the enzyme to the substrate and affect the catalytic action of the enzyme. $PMo_{11}Ni$ can bind to both the free enzyme and the enzyme-substrate complex, but this affects its inhibitory effect on α-glucosidase. Furthermore, Table 1 lists the inhibition constants (K_I and K_{IS}) of the four compounds for α-glucosidase.

3.2.3. Analysis of molecular docking results

In this part, we selected the best inhibitory compound $PMo_{11}Ni$ for α-glucosidase, and further researched the binding forms and interactions between $PMo_{11}Ni$ and α-glucosidase at the molecular level by molecular simulation, as shown in Fig. 2. The interactions between the ligand $PMo_{11}Ni$ and the most important amino acids generated by MOE are visualized in Fig. 2AC. The inhibitor perfectly matches to the active site pocket of α-glucosidase (Fig. 2AB), and the docking score was −13.35 kcal/mol after docking. The low score can be interpreted as measure for a strong enzyme-inhibitor binding and therefore as a reliable docking event.

In addition, $PMo_{11}Ni$ forms five hydrogen-bond interactions with the amino acid residues (Ser240, His280, Ser311, Pro312 and Arg315) in the active region (Fig. 2AC). $PMo_{11}Ni$ forms van der Waals interactions with the amino acid residues (Tyr158, Asp242, Leu246, Gln279, Asp307, Thr310, Leu313 and Phe314) around the active region (Fig. 2AC). In the docking interaction residue analysis, the four polar amino acids around the active binding site of the enzyme are Tyr158, Gln279, Asp307 and Thr310, respectively. These polar amino acid residues significantly contribute to the strong binding of the compound.

3.3. Analysis of vanadium-substituted Dawson-type POMs

3.3.1. Spectroscopic characterization

Elemental analysis (%): Anal. Calc. (Found) for $P_2Mo_{17}V$: P 1.80 (1.77), Mo 47.34 (47.23), V 1.48 (1.47); Anal. Calc. (Found) for $P_2Mo_{16}V_2$: P 1.80 (1.77), Mo 44.66 (44.54), V 2.91 (2.95); Anal. Calc. (Found) for $P_2Mo_{15}V_3$: P 1.74 (1.73), Mo 40.28 (40.17), V 4.28 (4.33); Anal. Calc. (Found) for $P_2Mo_{14}V_4$: P 1.81 (1.76), Mo 39.26 (39.29), V 5.96 (5.94) and Anal. Calc. (Found) for $P_2Mo_{13}V_5$: P 1.88 (1.83), Mo 37.73 (37.56), V 7.72 (7.70). These data results were consistent with the results of reference [37].

In addition, Table S5 listed the IR spectra (four characteristic bands at 700–1100 cm^{-1}) and the UV–*Vis* spectra (two characteristic absorption bands at 210 nm and 310 nm, repectively) data of the compounds $P_2Mo_{18-n}V_n$ (n = 1–5), and the ^{31}P NMR spectra was shown in Fig. S8. These data strongly indicated that these compounds were Dawson-type vanadium-substituted POMs, which was consistent with

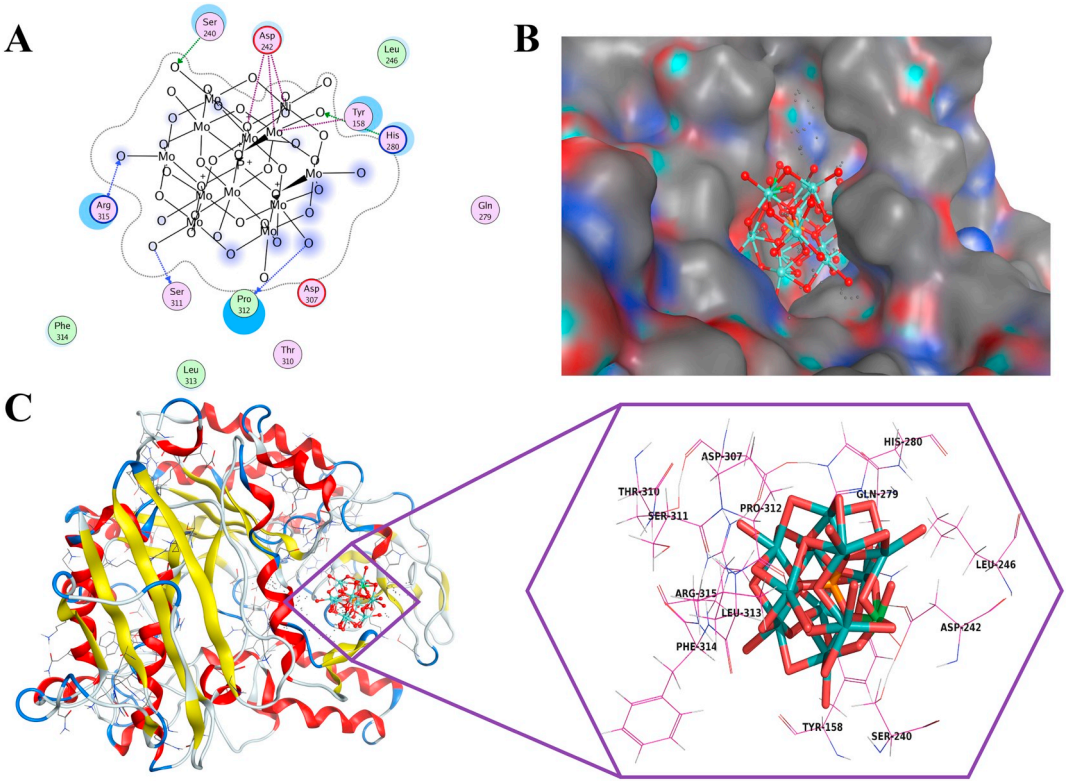

Fig. 2. Binding mode of the ligand $PMo_{11}Ni$ with α-glucosidase residues. (A) Two-dimensional ligand interaction map of compound $PMo_{11}Ni$ docked into the binding site of α-glucosidase. (B) The ligand $PMo_{11}Ni$ in the active site of α-glucosidase. (C) Three-dimensional complex interaction of ligand $PMo_{11}Ni$ with α-glucosidase residues.

the results of references [37, 38].

3.3.2. The inhibitory effect of compounds on α-glucosidase

Compared with Keggin-type structure, Dawson-type structure of POMs is relatively less studied and their redox ability is stronger. Therefore, a series of vanadium-substituted Dawson-type POMs were synthesized and used as inhibitors to study their inhibitory effects on α-glucosidase. As shown in Fig. S9, the α-glucosidase activity revealed a significant decrease with increased the concentrations of the inhibitors $P_2Mo_{18-n}V_n$ (n = 1–5). Comparing the IC_{50} of each compound (Table 1), it was found that the inhibitory effects of the five Dawson-type POMs on α-glucosidase were $P_2Mo_{17}V < P_2Mo_{14}V_4 < P_2Mo_{16}V_2 < P_2Mo_{13}V_5 < P_2Mo_{15}V_3$. It was revealed that, as compared to the acarbose (IC_{50} = 750 ± 1.5 μM) [44], the inhibition potency of $P_2Mo_{15}V_3$ (IC_{50} = 57.01 ± 2.11 μM) was approximately 13 times higher than that of acarbose, so the synthesized inhibitors possess significant inhibitory effects on α-glucosidase. Moreover, the V is easier reduced than the Mo, so that the Mo in the Dawson-type POMs is substituted by the V, and its oxidizability is markedly enhanced [37]. Therefore, we analyzed that the inhibitory effect of vanadium-substituted POMs on α-glucosidase is $P_2Mo_{17}V < P_2Mo_{16}V_2 < P_2Mo_{15}V_3$, because the increase in the number of vanadium substitutions may enhance the oxidizability of the compounds, which may indirect influence their binding affinities to the active site of the α-glucosidase. From this, it is speculated further that the inhibition of α-glucosidase is related to the elemental composition of the POMs, and the more the V-containing component (not more than three), the stronger the inhibitory effect on α-glucosidase. Similarly, we also found that the inhibition mechanisms of these five vanadium-substituted Dawson-type POMs are reversible (Fig. S10), and their inhibition types are all competitive (Fig. S11). In addition, Table 1 lists the inhibition constants (K_I) of these five compounds for α-glucosidase.

3.3.3. Analysis of molecular docking results

The above enzyme kinetics showed that the compound $P_2Mo_{15}V_3$ had the best inhibitory effect on α-glucosidase. Therefore, we further researched the binding forms and interactions of $P_2Mo_{15}V_3$ and α-glucosidase at the molecular level by the MOE (Fig. 3AB) and the PyMOL (Fig. 3C) software. As shown in Fig. 3AB, the $P_2Mo_{15}V_3$ accurately fit into the deep pocket of the active site and is largely surrounded by the polypeptide, and the docking score was −19.55 kcal/mol after docking. The low score can be interpreted as measure for a strong enzyme-inhibitor binding and therefore as a reliable docking event. Furthermore, $P_2Mo_{15}V_3$ forms six hydrogen bonds with the amino acid residues (Tyr158, Asp242, His280 and Ser311) in the active region (Fig. 3AC). In addition to the hydrogen-bond interactions with the enzyme, the compound also forms several van der Waals interactions which significantly contribute to the strong binding of the compound. $P_2Mo_{15}V_3$ forms van der Waals interactions with the amino acid residues (Val232, Ser240, Pro243, Leu246, Pro312, Leu313, Phe314 and Arg315) around the active region (Fig. 3AC). Similarly, in the docking interaction residue analysis, these polar amino acid residues (Ser240 and Arg315) significantly contribute to the strong binding of the compound.

4. Conclusions

In summary, to gain initial information about the structure-inhibition relationship of different POMs, three structural crucial factors of POMs - heteroatom, transition metal substitution element and vanadium substitution number - have been varied and the corresponding inhibition kinetics and molecular simulation performed. Enzyme kinetics demonstrated that our synthetic compounds PMo_{12} (6.41 ± 0.38 μM) [28], $PMo_{11}Ni$ (IC_{50} = 37.29 ± 1.72 μM) and $P_2Mo_{15}V_3$ (IC_{50} = 57.01 ± 2.11 μM) has the strongest inhibitory effect on α-glucosidase in their respective series, and their inhibitory effect was approximately 117, 20 and 13 times higher than that of standard

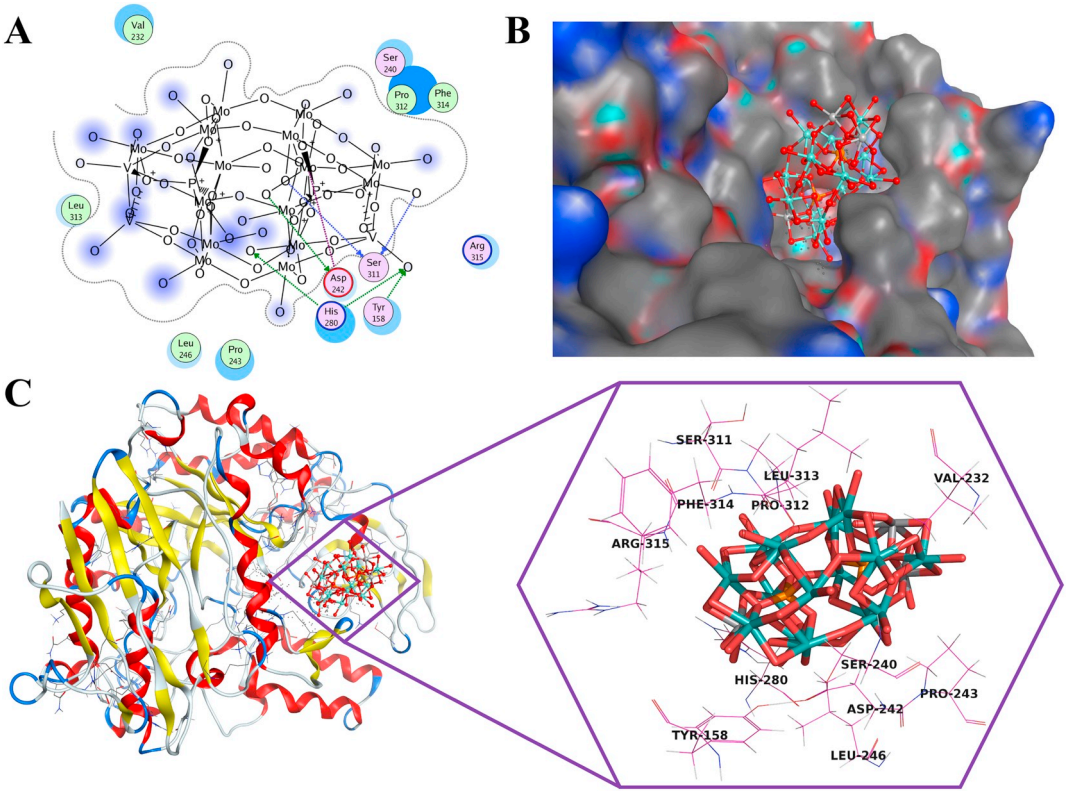

Fig. 3. Binding mode of the ligand $P_2Mo_{15}V_3$ with α-glucosidase residues. (A) Two-dimensional ligand interaction map of compound $P_2Mo_{15}V_3$ docked into the binding site of α-glucosidase. (B) The ligand $P_2Mo_{15}V_3$ in the active site of α-glucosidase. (C) Three-dimensional complex interaction of ligand $P_2Mo_{15}V_3$ with α-glucosidase residues.

acarbose, respectively. In addition, we found that all synthetic compounds except $PMo_{11}Ni$ (reversible mixed-type) and $PMo_{11}Fe$ (reversible noncompetitive) exhibited reversible competitive inhibition. Table 1 listed the inhibition constants (K_I and K_{IS}) of all compounds for α-glucosidase. More intriguingly, we found that the IC_{50} revealed a significant decrease with increased the heteropolyanions charge (Ga: −3, Si: −4 and P: −5), which indicated a significant indirect influence of the central atom charge on the inhibition behaviour. The structure and composition of POMs may change their own oxidation-reduction, acidity, and electrostatic effects of anion charge, which may also indirectly influence the inhibition behaviour of POMs on α-glucosidase. Moreover, molecular docking simulation demonstrated that the compounds we synthesized competitively bind to the active site of α-glucosidase mainly through multiple van-der-Waals and hydrogen bond interactions. The involvement of more polar amino acid residues significantly contributes to the strong binding of POMs on α-glucosidase. To some extent, molecular simulations validated the experimental results of enzyme kinetics, and further expound upon the mechanisms of action at the molecular level. Through future experiments, we will further study the effects of factors such as counter cations and lattice water on the structure-activity relationship of POMs, and further expand our investigation with the human α-glucosidase and the model enzyme isomaltase. Furthermore, we will determine the X-ray structure of α-glucosidase-POMs complex for comparison and for evaluating the accuracy of the modeling data. In this sense, this work further advances our understanding of the design and synthesis of POMs as therapeutic agents for type 2 diabetes. Also, this work opens up a window toward the biomedical applications of polyoxometalate chemistry.

Supplementary data to this article can be found online at https://doi.org/10.1016/j.jinorgbio.2019.110784.

Acknowledgements

This work was supported by the National Natural Science Foundation of China (Grant No. 21871110) and the National Key Research and Development Program of China (Grant No. 2018YFD0901004).

References

[1] S.H. Ley, A.V. Ardisson Korat, Q. Sun, D.K. Tobias, C. Zhang, L. Qi, W.C. Willett, J.E. Manson, F.B. Hu, Contribution of the nurses' health studies to uncovering risk factors for type 2 diabetes: diet, lifestyle, biomarkers, and genetics[J], Am. J. Public Health 106 (9) (2016) 1624–1630, https://doi.org/10.2105/AJPH.2016.303314.
[2] A. Migdal, M. Abrahamson, A. Peters, N. Vint, Approaches to rapid acting insulin intensification in patients with type 2 diabetes mellitus not achieving glycemic targets[J], Ann. Med. (2018) 1–27, https://doi.org/10.1080/07853890.2018.1493216.
[3] D.N. Olennikov, N.K. Chirikova, N.I. Kashchenko, V.M. Nikolaev, S.W. Kim, C. Vennos, Bioactive phenolics of the genus artemisia (asteraceae): HPLC-DAD-ESI-TQ-MS/MS profile of the siberian species and their inhibitory potential against α-amylase and α-glucosidase[J], Front. Pharmacol. 9 (2018) 756–783, https://doi.org/10.3389/fphar.2018.00756.
[4] X. Peng, G. Zhang, Y. Liao, D. Gong, Inhibitory kinetics and mechanism of kaempferol on α-glucosidase[J], Food Chem. 190 (2016) 207–215, https://doi.org/10.1016/j.foodchem.2015.05.088.
[5] M. Taha, S.A.A. Shah, M. Afifi, S. Imran, S. Sultan, F. Rahim, K.M. Khan, Synthesis, α-glucosidase inhibition and molecular docking study of coumarin based derivatives[J], Bioorg. Chem. 77 (2018) 586–592, https://doi.org/10.1016/j.bioorg.2018.01.033.
[6] S.P. Clissold, C. Edwards, Acarbose: a preliminary review of its pharmacodynamic and pharmacokinetic properties, and therapeutic potential[J], Drugs 35 (3) (1988) 214–243, https://doi.org/10.2165/00003495-198835030-00003.
[7] L.J. Scott, C.M. Spencer, Miglitol: a review of its therapeutic potential in type 2 diabetes[J], Drugs 59 (3) (2000) 521–549, https://doi.org/10.2165/00003495-200059030-00012.
[8] K. Kaku, Efficacy of voglibose in type 2 diabetes[J], Expert. Opin. Pharmacother. 15 (8) (2014) 1181–1190, https://doi.org/10.1517/14656566.2014.918956.
[9] A. Bijelic, M. Aureliano, A. Rompel, Polyoxometalates as potential next-generation

metallodrugs in the combat against cancer[J], Angew. Chem. Int. Ed. 57 (2018) 2–22, https://doi.org/10.1002/anie.201803868.
[10] R. Francese, A. Civra, M. Rittà, M. Donalisio, M. Argenziano, R. Cavalli, A. Mougharbel, U. Kortz, D. Lembo, Anti-zika virus activity of polyoxometalates, [J]. Antivir. Res. 163 (2019) 29–33, https://doi.org/10.1016/j.antiviral.2019.01.005.
[11] L. Pérez-Álvarez, L. Ruiz-Rubio, B. Artetxe, M. dM Vivanco, J.M. Gutiérrez-Zorrilla, J.L. Vilas-Vilela, Chitosan nanogels as nanocarriers of polyoxometalates for breast cancer therapies[J], Carbohydr. Polym. 213 (2019) 159–167, https://doi.org/10.1016/j.carbpol.2019.02.091.
[12] X.H. Li, W.L. Chen, M. Wei, J. Liu, Y. Di, L. Liu, E.B. Wang, Polyoxometalates nanoparticles improve anti-tumor activity by maximal cellular uptake[J], Inorg. Chim. Acta 486 (2019) 104–112, https://doi.org/10.1016/j.ica.2018.10.046.
[13] J. Liu, W.J. Mei, A.W. Xu, C.P. Tan, S. Shi, L.N. Ji, Synthesis, characterization and antiviral activity against influenza virus of a series of novel manganese-substituted rare earth borotungstates heteropolyoxometalates[J], Antivir. Res. 62 (1) (2004) 65–71, https://doi.org/10.1016/j.antiviral.2003.12.004.
[14] A. Bijelic, M. Aureliano, A. Rompel, The antibacterial activity of polyoxometalates: structures, antibiotic effects and future perspectives[J], Chem. Commun. 54 (10) (2018) 1153–1169, https://doi.org/10.1039/c7cc07549a.
[15] D. Marques-da-Silva, G. Fraqueza, R. Lagoa, A.A. Vannathan, S.S. Mal, M. Aureliano, Polyoxovanadates inhibition of *Escherichia coli* growth shows a reverse correlation with Ca^{2+}-ATPase inhibition[J], New J. Chem. (2019), https://doi.org/10.1039/C9NJ01208G.
[16] M. Ma, N. Gao, Y. Sun, X. Du, J. Ren, Qu, X. Redox-activated near-infrared-responsive polyoxometalates used for photothermal treatment of Alzheimer's disease [J], Adv. Healthc. Mater. (2018) e1800320, , https://doi.org/10.1002/adhm.201800320.
[17] N. Gao, K. Dong, A. Zhao, H. Sun, Y. Wang, J. Ren, X. Qu, Polyoxometalate-based nanozyme: design of a multifunctional enzyme for multi-faceted treatment of Alzheimer's disease[J], Nano Res. 9 (4) (2016) 1079–1090, https://doi.org/10.1007/s12274-016-1000-6.
[18] N. Gao, H. Sun, K. Dong, J. Ren, T. Duan, C. Xu, X. Qu, Transition-metal-substituted polyoxometalate derivatives as functional anti-amyloid agents for Alzheimer's disease[J], Nat. Commun. 5 (2014) 3422, https://doi.org/10.1038/ncomms4422.
[19] S.Y. Lee, A. Fiene, W. Li, T. Hanck, K.A. Brylev, V.E. Fedorov, J. Lecka, A. Haider, H. Pietzsch, H. Zimmermann, J. Sévigny, U. Kortz, H. Stephan, C.E. Müller, Polyoxometalates-potent and selective ecto-nucleotidase inhibitors[J], Biochem. Pharmacol. 93 (2) (2015) 171–181, https://doi.org/10.1016/j.bcp.2014.11.002.
[20] W. Liu, R. Al-Oweini, K. Meadows, B.S. Bassil, Z. Lin, J.H. Christian, N.S. Dalal, A.M. Bossoh, I.M. Mbomekallé, P. de Oliveira, J. Iqbal, Cr^{III}-substituted heteropoly-16-tungstates $[Cr_2^{III}(B\text{-}\beta\text{-}X^{IV}W_8O_{31})_2]^{14-}$ (X = Si, Ge): magnetic, biological, and electrochemical studies[J], Inorg. Chem. 55 (21) (2016) 10936–10946, https://doi.org/10.1021/acs.inorgchem.6b01458.
[21] M. Arefian, M. Mirzaei, H. Eshtiagh-Hosseini, A. Frontera, A survey of the different roles of polyoxometalates in their interaction with amino acids, peptides and proteins[J], Dalton Trans. 46 (21) (2017) 6812–6829, https://doi.org/10.1039/C7DT00894E.
[22] G. Fraqueza, J. Fuentes, L. Krivosudský, S. Dutta, S.S. Mal, A. Roller, M. Aureliano, Inhibition of Na^+/K^+-and Ca^{2+}-ATPase activities by phosphotetradecavanadate [J], J. Inorg. Biochem. 197 (2019) 110700, , https://doi.org/10.1016/j.jinorgbio.2019.110700.
[23] H. Stephan, M. Kubeil, F. Emmerling, C.E. Müller, Polyoxometalates as versatile enzyme inhibitors[J], Eur. J. Inorg. Chem. 2013 (10−11) (2013) 1585–1594, https://doi.org/10.1002/ejic.201201224.
[24] N. Gumerova, L. Krivosudský, G. Fraqueza, J. Breibeck, E. Al-Sayed, E. Tanuhadi, A. Bijelic, J. Fuentes, M. Aureliano, A. Rompel, The P-type ATPase inhibiting potential of polyoxotungstates[J], Metallomics 10 (2018) 287–295, https://doi.org/10.1039/c7mt00279c.
[25] B. Hasenknopf, Polyoxometalates: introduction to a class of inorganic compounds and their biomedical applications[J], Front. Biosci. 10 (2005) 275–287, https://doi.org/10.2741/1527.
[26] E. Sánchez-Lara, S. Treviño, B.L. Sánchez Gaytán, E. Sánchez-Mora, M.E. Castro, F.J. Meléndez-Bustamante, ... E. González-Vergara, Decavanadate salts of cytosine and metformin: a combined experimental-theoretical study of potential metallodrugs against diabetes and cancer[J], Front. Chem. 6 (2018) 402, , https://doi.org/10.3389/fchem.2018.00402.
[27] Z. Ilyas, H.S. Shah, R. Al-Oweini, U. Kortz, J. Iqbal, Antidiabetic potential of polyoxotungstates: *in vitro* and *in vivo* studies[J], Metallomics 6 (8) (2014) 1521–1526, https://doi.org/10.1039/C4MT00106K.
[28] G. Chi, Y. Qi, J. Li, L. Wang, J. Hu, Polyoxomolybdates as α-glucosidase inhibitors: kinetic and molecular modeling studies[J], J. Inorg. Biochem. 193 (2019) 173–179, https://doi.org/10.1016/j.jinorgbio.2019.02.001.
[29] Y. Qi, Y. Xiang, J. Wang, Y. Qi, J. Li, J. Niu, J. Zhong, Inhibition of hepatitis C virus infection by polyoxometalates[J], Antivir. Res. 100 (2) (2013) 392–398, https://doi.org/10.1016/j.antiviral.2013.08.025.
[30] J. Geng, M. Li, J. Ren, E. Wang, X. Qu, Polyoxometalates as inhibitors of the aggregation of amyloid β peptides associated with Alzheimer's disease[J], Angew. Chem. Int. Ed. 50 (18) (2011) 4184–4188, https://doi.org/10.1002/ange.201007067.
[31] Z. Han, E. Wang, G. Luan, Y. Li, H. Zhang, Y. Duan, C. Hua, N. Hu, Synthesis, properties and structural characterization of an intermolecular photosensitive complex: $(HGly\text{-}Gly)_3PMo_{12}O_{40}\cdot 4H_2O$[J], J. Mater. Chem. 12 (4) (2002) 1169–1173, https://doi.org/10.1039/B107225K.
[32] Q. Wu, J. Wang, L. Zhang, A. Hong, J. Ren, Molecular recognition of basic fibroblast growth factor by polyoxometalates[J], Angew. Chem. Int. Ed. Engl. 44 (26) (2005) 4048–4052, https://doi.org/10.1002/anie.200500108.
[33] L.P. Tsiganok, A.B. Vishnikin, R.I. Maksimovskaya, UV, IR, ^{71}Ga and ^{17}O NMR spectroscopic studies of the 12-molybdogallate heteropolyanion[J], Polyhedron 8 (23) (1989) 2739–2742, https://doi.org/10.1016/S0277-5387(00)80529-X.
[34] C. Rocchiccioli-Deltcheff, M. Fournier, R. Franck, R. Thouvenot, Vibrational investigations of polyoxometalates. 2. Evidence for anion-anion interactions in molybdenum (VI) and tungsten (VI) compounds related to the Keggin structure[J], Inorg. Chem. 22 (2) (1983) 207–216, https://doi.org/10.1021/ic00144a006.
[35] M. Lapkowski, W. Turek, M. Barth, S. Lefrant, Changes in catalytic properties of substituted and unsubstituted heteropolyacids in conductive polymer matrix[J], Synth. Met. 69 (1–3) (1995) 127–128, https://doi.org/10.1016/0379-6779(94)02386-D.
[36] T. Mazari, C.R. Marchal, S. Hocine, N. Salhi, C. Rabia, Oxidation of propane over substituted Keggin phosphomolybdate salts[J], J. Nat. Gas Chem. 18 (3) (2009) 319–324, https://doi.org/10.1016/S1003-9953(08)60111-5.
[37] E.B. Wang, L.H. Gao, J.F. Liu, Z.X. Liu, D.H. Yan, Preparation and properties of the molybdovanadophosphoric acids with Dawson structure[J], Acta Chim. Sin. 46 (8) (1988) 757–762.
[38] S. Jing, Z. Wang, W. Zhu, J. Guan, G. Wang, Oxidation of cyclohexane with hydrogen peroxide catalyzed by Dawson-type vanadium-substituted heteropolyacids [J], React. Kinet. Catal. Lett. 89 (1) (2006) 55–61, https://doi.org/10.1007/s11144-006-0086-3.
[39] C. Scholz, S. Knorr, K. Hamacher, B. Schmidt, DOCKTITE-a highly versatile step-by-step workflow for covalent docking and virtual screening in the molecular operating environment[J], J. Chem. Inf. Model. 55 (2) (2015) 398–406, https://doi.org/10.1021/ci500681r.
[40] M.S. Islam, A. Barakat, A.M. Al-Majid, M. Ali, S. Yousuf, M.I. Choudhary, R. Khalil, Z. UI-Haq, Catalytic asymmetric synthesis of indole derivatives as novel α-glucosidase inhibitors *in vitro*[J], Bioorg. Chem. 79 (2018) 350–354, https://doi.org/10.1016/j.bioorg.2018.05.004.
[41] M. Taha, N.H. Ismail, S. Imran, A. Wadood, M. Ali, F. Rahim, A.A. Khan, M. Riaz, Novel thiosemicarbazide-oxadiazole hybrids as unprecedented inhibitors of *yeast* α-glucosidase and in silico binding analysis[J], RSC Adv. 6 (40) (2016) 33733–33742, https://doi.org/10.1039/C5RA28012E.
[42] M.T. Pope, Heteropoly and Isopoly Oxometalates[J], Springer-Verlag, 1983.
[43] M.N. Timofeeva, Acid catalysis by heteropoly acids[J], Appl. Catal. A Gen. 256 (1–2) (2003) 19–35, https://doi.org/10.1016/S0926-860X(03)00386-7.
[44] M. Mohammadi-Khanaposhtani, S. Rezaei, R. Khalifeh, S. Imanparast, M.A. Faramarzi, S. Bahadorikhalili, M. Safavi, F. Bandarian, E.N. Esfahani, M. Mahdavi, B. Larijani, Design, synthesis, docking study, α-glucosidase inhibition, and cytotoxic activities of acridine linked to thioacetamides as novel agents in treatment of type 2 diabetes[J], Bioorg. Chem. 80 (2018) 288–295, https://doi.org/10.1016/j.bioorg.2018.06.035.
[45] R. Xing, A. Zheng, F. Wang, L. Wang, Y. Yu, A. Jiang, Functionality study of $Na_6PMo_{11}FeO_{40}$ as a mushroom tyrosinase inhibitor[J], Food Chem. 175 (2015) 292–299, https://doi.org/10.1016/j.foodchem.2014.11.157.